



Cite this: *Soft Matter*, 2015,
11, 7953

Oxygen reduction reaction induced pH-responsive chemo-mechanical hydrogel actuators†

Cunjiang Yu,‡^a Peixi Yuan,‡^b Evan M. Erickson,^b Christopher M. Daly,^b
John A. Rogers*^a and Ralph G. Nuzzo*^b

We describe and characterize elementary designs for electrochemical micro- and macro-scale chemomechanical hydrogel actuators. The actuation of a pH-sensitive cross-linked polyacrylic acid (PAA) hydrogel is driven in the model devices through the oxygen reduction reaction (ORR) occurring at the electrodes of an embedded Au mesh micro-electrochemical array. Proton consumption by the ORR at the cathode of the embedded electrochemical cell leads to the formation of a localized pH gradient that in turn drives the strain response in the composite actuators. The dynamics result from the ionization of the carboxylic acid moieties of the PAA network in the high pH region, yielding an osmotic pressure that drives a volumetric expansion due to water imbibition. This system actuates both stably and reversibly; when the electrochemically-induced ORR is halted, the localized pH gradient dissipates due to diffusive mixing, which in turn relaxes the induced strains. Two approaches to the fabrication of hydrogel actuators were examined in this work. The first method adopted a design based on small flagella ($\sim 0.2 \text{ mm} \times 1.5 \text{ mm} \times 60 \text{ }\mu\text{m}$, width \times length \times height) in which the actuating PAA structures are molded atop a set of fixed electrodes mounted on a supporting substrate. These hydrogel actuators show fast, large-amplitude, and largely reversible responses in the ORR mediated chemomechanical dynamics. We also investigated larger hydrogel actuators ($\sim 4.5 \text{ mm} \times 11 \text{ mm} \times 1 \text{ mm}$, width \times length \times height), based on an autonomous design that embeds an open mesh stretchable micro-electrode array within the hydrogel. The significant and design-dependent impacts of mass transfer on the chemomechanical dynamics are evidenced in each case, a feature examined to elucidate more efficient mesoscopic design rules for actuators of this form.

Received 29th July 2015,
Accepted 24th August 2015

DOI: 10.1039/c5sm01892g

www.rsc.org/softmatter

1. Introduction

The literature demonstrates a growing interest in the design of soft material systems and devices that engender possibilities for programmable forms of mechanical actuation. All systems of this type require some form of energy conversion, and a means for integrating that feature with a stimuli-responsive (*e.g.* polymeric) material. The useful forms for such materials include applications ranging from simple mechanical actuators^{1,2} to sophisticated integrated systems as found in soft robotics.^{3,4} The mechanics of interest in materials of this type can be quite varied and include deformation,⁴ volume change,⁵ changes in modulus,⁶ and driven motion,⁷ among others. Numerous mechanisms to trigger these responses have been investigated and, for soft-material actuators, temperature,⁸ pH,⁹ electric

field,¹⁰ ion concentration,¹¹ and chemical or biological reagents^{12,13} have emerged as garnering the greatest interest. Of these, electric-field-driven mechanisms appear to be one of the most straightforward and attractive triggers for realizing a muscle-like actuator.^{4,14,15}

The current work is centered on the development of, and the elucidation of principles for the efficient operation of, soft-actuators that are chemomechanically driven. In an earlier report, we examined a simple gel-based soft actuator that engendered capacities for programmed/deterministic modes of mechanical actuation.¹⁶ This device design utilized an embedded micro mesh electrode to drive spatially programmable thermal phase transformations in a poly-*N*-isopropylacrylamide (pNIPAM) soft material actuator. The conformational transitions so engendered allowed fully programmable forms of actuation. The current study extends this work, using the embedded micro mesh electrode design as an electrochemical micro reactor rather than a simple resistive heater as in the previous work. We use this capacity here as a means to localize pH gradients, *via* small Faradaic currents attending the oxygen-reduction-reaction (ORR), in the vicinity of soft, pH-responsive, gel structures. In previous studies,^{17–19} we demonstrated substantial, stable, pH gradients in a microfluidic channel

^a Department of Materials Science and Engineering, University of Illinois-Urbana Champaign, Urbana, Illinois 61801, USA. E-mail: jrogers@illinois.edu

^b School of Chemical Sciences, University of Illinois-Urbana Champaign, Urbana, Illinois 61801, USA. E-mail: r-nuzzo@illinois.edu

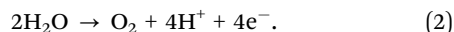
† Electronic supplementary information (ESI) available. See DOI: 10.1039/c5sm01892g

‡ Equal contribution.

with the ORR driven electrochemically. This specific electrochemical reaction is suitable for microfluidic channels or, as is shown in this work, for direct integration into hydrogel actuators because no undissolved gas—which would cause bubbling inside the electrochemical cell—is produced by the ORR.¹⁸ In acidic media, the ORR consumes protons at the cathode, according to the following reaction:²⁰



The anode produces protons and oxidizes water or other liquid species, giving oxygen as a product of the former:²⁰



The overall process therefore generates localized pH gradients between the cathode (higher pH) and the anode (lower pH), which drives ionization changes in pH-sensitive hydrogels, such as the PAA used in this work. In the higher pH environment, the protonated carboxylic acid moieties of PAA are ionized, producing an osmotic pressure gradient in the hydrogel relative to the external solution, which drives an expansion of the PAA actuator.²¹ We show here that the mechanical actuation so effected is reversible due to subsequent diffusive dissipation of the pH gradient after stopping the ORR.

In this work, we fabricated both micro- and macro-scale composite hydrogel actuators consisting of PAA hydrogel embedded with Au electrochemical arrays. In the micro-scale actuator, the small hydrogel dimensions ($\sim 0.2 \text{ mm} \times 1.5 \text{ mm} \times 60 \mu\text{m}$, width \times length \times height), enable quicker stimuli responses as well as larger, and more promptly reversible, chemomechanical actuation. To demonstrate this actuation in larger dimensions, a macro-scale composite actuator ($\sim 4.5 \text{ mm} \times 11 \text{ mm} \times 1 \text{ mm}$, width \times length \times height) was fabricated with open mesh stretchable electrodes embedded into the PAA hydrogel network. In both systems, the ORR current generates localized pH gradients, with tunable temporal and spatial attributes, that drive chemomechanical actuation in the composite system. Dissipation of the pH gradients, due to diffusive mixing after the ORR current is stopped, removes the induced strains, relaxing the actuator nearly back to its original state. The strains induced are strongly scale dependent, with the largest strain amplitudes being manifested at the mesoscale limit of small system dimensions. We discuss this point in greater detail in an analysis of designs that can enhance the efficiency of this form of chemomechanical actuation.

2. Experimental

2.1 Materials

All chemicals were used as received without purification unless otherwise noted: acrylic acid (Sigma-Aldrich, 99%), acrylamide (Acros Organics, 99%), methylenebisacrylamide (Sigma-Aldrich, 99%), Darocure 1173 (Ciba), methacryloxyethyl thiocarbonyl rhodamine B (polysciences, Inc.), potassium chloride (Sigma-Aldrich, 99%), PDMS (Sylgard 184, Dow Corning), silicon wafer ((100), University Wafer).

2.2 Synthesis of the hydrogel pre-gel solutions

2.2.1 Synthesis of PAA. The pre-gel solution mixture was prepared by dissolving acrylic acid (175 mg, 2.4 mM), *N,N'*-methylenebis acrylamide (20 mg, 0.03 mM), and Darocur 1173 (30 μL , 1.8×10^{-4} mM) in DMSO and H_2O (1 mL, 1:1, DMSO: H_2O by volume). For the micro-scale actuator, the pre-gel solution was injected into a microfluidic channel (detailed fabrication procedure in Section 2.3), and irradiated with 365 nm UV light for 60 seconds to polymerize (exposure dose $\sim 350 \text{ mJ cm}^{-2}$). For the macro-scale actuator, pre-gel solution was poured into a square shaped container with 2 cm edge length and photopolymerized with the stretchable electrode under the 365 nm UV light, (detailed fabrication procedure in Section 2.4).

2.2.2 Synthesis of PAAM. The pre-gel solution mixture was prepared by dissolving acrylamide (175 mg, 2.5 mM), *N,N'*-methylenebis acrylamide (20 mg, 0.03 mM), and Darocur 1173 (30 μL , 1.8×10^{-4} mM) in DMSO and H_2O (1 mL, 1:1, DMSO: H_2O by volume).

2.3 Fabrication of the microfluidic channel mold

The PDMS microfluidic channel mold was fabricated by soft lithography as reported elsewhere.¹⁹ Negative photoresist (PR) SU8-50 was spin-coated on a 2 inch diameter silicon wafer (1750 rpm, 30 seconds, thickness $\sim 60 \mu\text{m}$). The SU8-50 was irradiated with 365 nm UV light at a dose of 500 mJ cm^{-2} and then developed to generate the desired pattern, which served as a mold. Degassed PDMS (10:1 ratio, Sylgard 184) mixture was poured onto the patterned mold in a 2 inch diameter Petri dish. After curing the PDMS at $70 \text{ }^\circ\text{C}$ in an oven for 2 hours, the PDMS mold is cut and peeled away from the silicon wafer.

2.4 Fabrication of the electrodes for the micro PAA actuator

Glass slides (5 cm \times 7 cm) were cleaned in piranha solution. Negative PR AZ 5214 was used for metal electrode lift-off on the glass slides. Specifically, PR AZ2020 was spin coated at 3000 rpm for 30 seconds, followed by soft bake and photopatterning. After developing the photoresist to generate the desired patterns, 5/250 nm thick titanium (Ti) and gold (Au) were deposited. The metal electrode was completed by lift-off in acetone while removing any remaining PR.

2.5 Electrochemical measurements

The electrochemical measurements were performed in a solution of 0.1 M KCl at pH = 4, using CHI 650B electrochemistry workstation (CH Instrument, Austin, Texas, USA). The CV was taken in the same micro actuator cell used to analyze the micro PAA actuator but without the gel. Both cathode and anode are Au and the CV measurements were made open to air at a scan rate of 20 mV s^{-1} . A 2-electrode system was used in the electrochemical experiments, considering the Au electrode on the anode as a pseudo-reference electrode. As shown in ESI,† Fig. S1, this system has the same CV pattern as a 3 electrode system (*vs.* Ag/AgCl), under which the system reduces oxygen at -0.2 V (*vs.* Ag/AgCl), with a potential shift of -0.95 V for the pseudo-reference case (ESI,† Section I).

3. Results and discussion

3.1 Fabrication of the micro PAA actuator

The process steps for the fabrication of the micro-scale actuator are depicted schematically in Fig. 1a. By adhering the PDMS microfluidic channel mold (from Section 2.3) onto the fabricated electrode array, a covered microfluidic channel system was formed. The PAA pre-gel solution was injected into the microfluidic channel and covered by a photomask with desired patterns. The device was irradiated with 365 nm UV light (exposure dose $\sim 350 \text{ mJ cm}^{-2}$). An optical image of the fabricated PAA micro strips is shown in Fig. 1b. The cathode ends of the strips were then covered with a shorter microfluidic channel network which served to anchor the strips to the substrate. A set of PDMS blocks were then laid around electrodes, on top of the substrate surface, as a reservoir to contain the electrolyte. Electrolyte solution (0.1 M KCl, pH = 4.0) was applied to ensure that the micro strip arrays were fully immersed. Finally, a thin blade was used to release the free ends of the PAA micro strips from the substrate. The latter delamination of the gel allows the PAA micro strips to swell and deswell freely in the contacting electrolyte solution.

3.2 Fabrication of the macro PAA actuator

One of the key design considerations for the stretchable electrodes of this actuator includes minimizing the mechanical constraints they impose on the more easily deformed hydrogel component. For this reason, the electrode was designed as thin serpentine shapes that are mechanically stretchable and compressible, following strategies that have been extensively studied in stretchable electronics.¹⁶ The electrode mesh has an overall dimension of $3.3 \text{ mm} \times 10 \text{ mm}$, and it contains four separate serpentine shaped electrodes (Fig. S2a, ESI[†]). The width of the metal electrode is $60 \mu\text{m}$, and the width of the polyimide (PI) supporting structure is $120 \mu\text{m}$

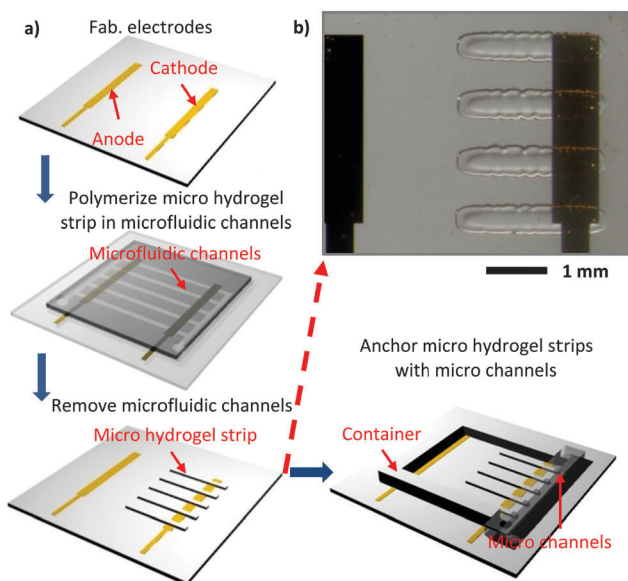


Fig. 1 (a) Schematic illustration of the fabrication procedures for the micro PAA actuator with the coupled micro-electrode array. (b) Optical image of the fabricated micro PAA actuator.

(Fig. S2b and c, ESI[†]). A lithographic patterning step is used to expose the Au for electrolyte contact through channels placed along electrode length (discussed in greater detail in ESI[†], Section II).

To integrate the electrode mesh into the hydrogel component, the electrode mesh (as prepared in ESI[†], Section II) was embedded into the hydrogel by alignment and photo curing under a mask aligner (Karl Suss, MJB3). Fig. 2a illustrates the schematic steps for this embedding process. Specifically, the electrode mesh was placed in a container, and the gel precursor solution was added with the mesh being suspended in the solution.

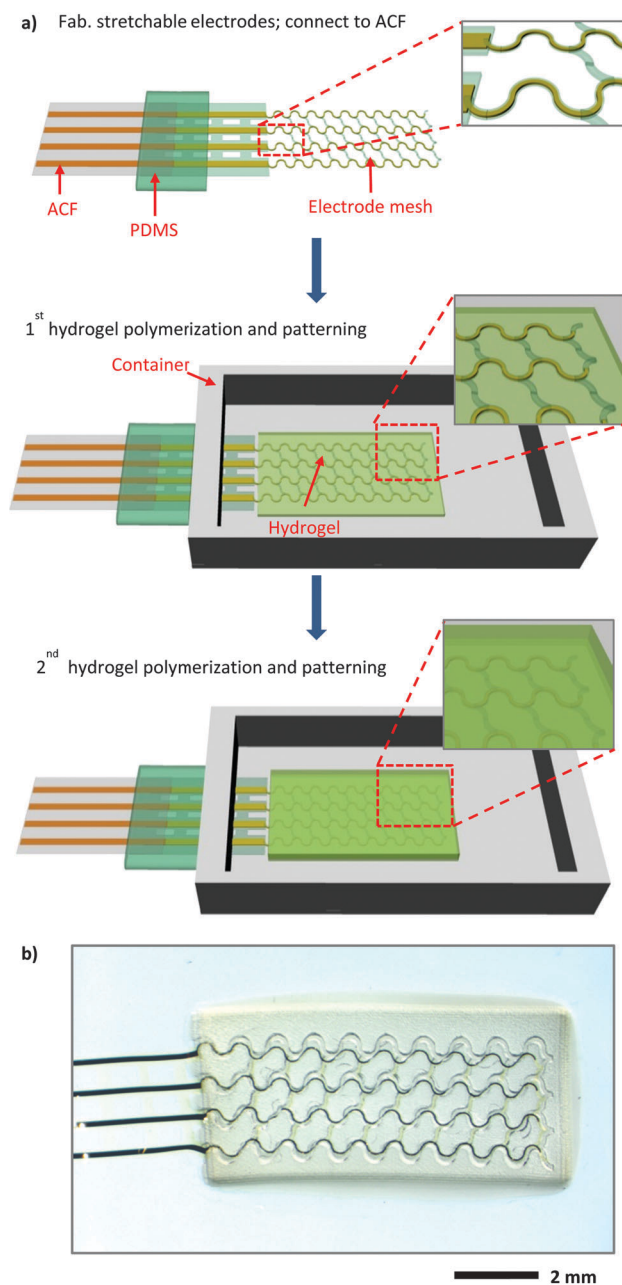


Fig. 2 (a) Schematic illustration of the fabrication of the macro PAA actuator with open mesh embedded stretchable electrodes. (b) Optical image of the macro PAA actuator in aqueous solution.

After aligning the electrode with a photomask, the hydrogel was formed by polymerization under ultra violet (UV) light. Following the removal of the remaining unpolymerized solution, another layer of hydrogel was further polymerized by repeating the previous steps. The actuator was formed by sandwiching the stretchable electrodes with two layers of the hydrogels, as shown in Fig. 2b, and immersing the material in water to remove excess materials (*e.g.* monomer and initiator species) retained within them.

3.3 ORR-induced chemomechanics of the micro PAA actuator

For the fabrication sequence described above, the dimensions of the hydrogel cilia affixed in the micro PAA actuator were $200\ \mu\text{m} \times 1.5\ \text{mm} \times 60\ \mu\text{m}$ (width \times length \times thickness). The actuation of these structures by the ORR (Fig. 3) was performed at potential $-1.15\ \text{V}$ (*vs.* Au pseudo-reference) in a $0.1\ \text{M}$ KCl ($\text{pH} = 4$) electrolyte (explained in ESI,† Section I). Immersed in this electrolyte, the PAA cilia swell to an average length of $2.48\ \text{mm}$ at equilibrium before subjected to the influences of the co-localized ORR (Fig. 3a-i). After 30 minutes of electrolysis, the PAA micro strips were seen to swell (Fig. 3a-ii) to an average length of $3.50\ \text{mm}$. Removing the applied potential, the PAA micro strips gradually relaxed to dimensions close to their original size (average length $\sim 2.53\ \text{mm}$, Fig. 3a-iii). ESI,† Section III (Fig. S3, ESI†) provides information about the temporal

programming used to test the system. The plot in Fig. 3b shows strain changes seen in the micro PAA actuator through three cycles of actuation. The induced strains, ε , are given by the following equation:

$$\varepsilon = \frac{L_0 - L}{L_0} \times 100\% \quad (3)$$

where L_0 is the original length of the cilia before initiation of the ORR and L is the contour length at the time of measurement. In each cycle, the PAA micro strips sustain a consistent, largely reversible, maximum strain of nearly 40% (ESI,† Movie S1), demonstrating the effects arising from a significant localized pH gradient between the cathode and anode. The consumption of protons at the cathode, because of its proximate placement, ionizes the PAA of the cilia which in turn causes the volumetric expansion of the hydrogel component. Ceasing the ORR causes diffusive dissipation of the pH gradient with a subsequent reversion of the chemomechanical state of the PAA micro strips (ESI,† Movie S2).

3.4 Design variables influencing the efficiency of the micro PAA actuator dynamics

In this system, we found that inter-electrode distance and ORR current magnitudes are the significant factors for PAA actuation (Fig. 4). These variables were optimized in PAA micro strips ($400\ \mu\text{m}$ wide) to obtain maximal actuation responses from the

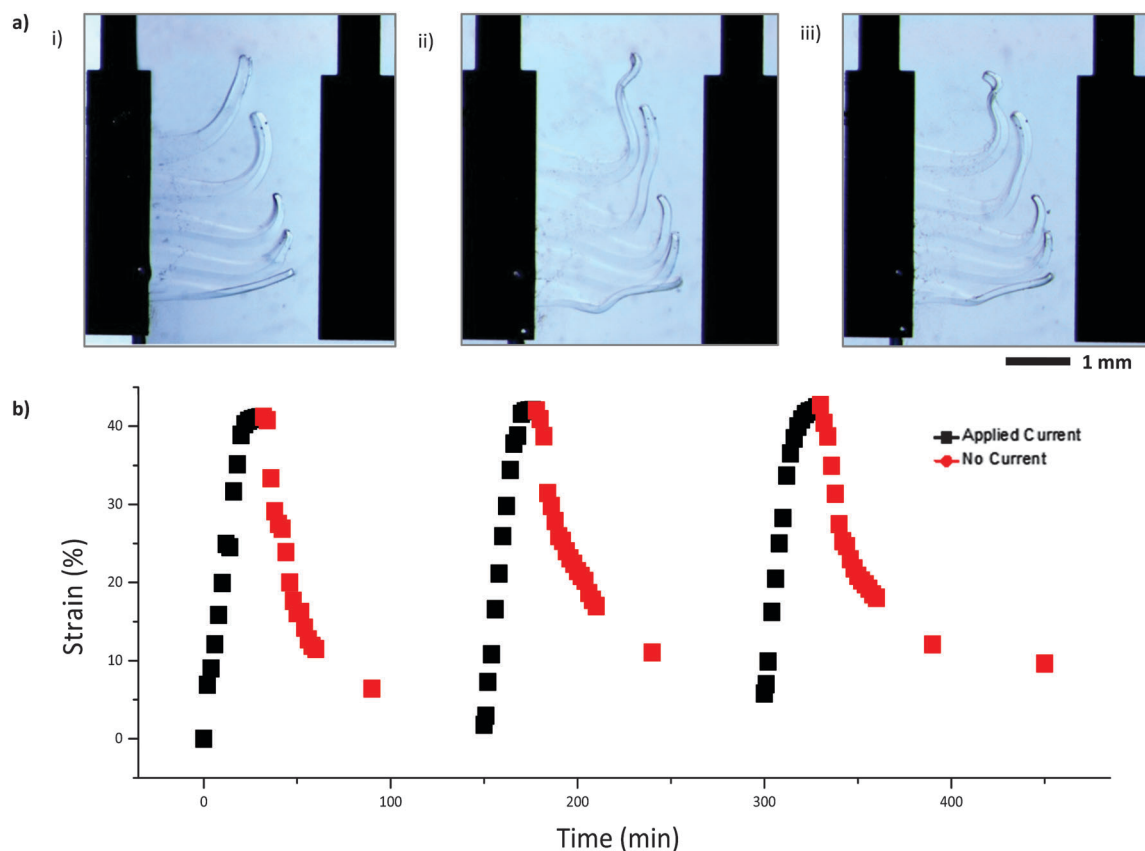


Fig. 3 (a) Optical image of micro PAA actuator immersed in electrolyte solution ($0.1\ \text{M}$ KCl, $\text{pH} = 4.0$) (i) before application of ORR current, (ii) after application of ORR current for 30 minutes, and (iii) after removal of ORR current for 60 minutes. The distance between electrodes is $3\ \text{mm}$. (b) Graphical illustration of strain change in the micro PAA actuator through three cycles of applying and removing the ORR current.

electrochemical to mechanical energy conversion. Fig. 4a (experimental images in Fig. S4, ESI[†]) tracks the strain change seen for PAA micro strips at varied inter-electrode distances, here ranging from 3 mm to 12 mm, at constant current magnitudes (6 μA). The samples with inter-electrode distances of 3, 6, and 12 mm had maximum strains of 32.7%, 24.8%, and 17.1%, respectively. These results indicate that a smaller inter-electrode distance induces a more effective pH gradient for the same number of electrons passed in the electrolytic processes.

It is important to note that the dissipative dynamics that drive the actuation in this system are in fact subject to dissipative losses, that the strain states developed in the gel reflect on both aspects of kinetics (ones that are electrochemical and gel-centric in their nature) and the dissipation of the sustaining gradient due to diffusive loss to the background electrolyte. In principle, the hydroxide flux created at the cathode is likely balanced by a compensating (and proton forming) reaction occurring at the anode. In our earlier work, we did in fact find that such compensating gradients were formed at the embedded electrodes of a microcapillary-based micro-electrochemical reactor. We have not established, however, that the processes occurring at each electrode here are fully balanced, that each mediates the observed pH gradient *via* an ORR process that is selectively compensated by a water oxidation reaction occurring at the anode. At higher current densities, bubbles are evidenced due to the latter reaction. Still it remains that competing pathways might lead to inefficiencies that limit actuation.

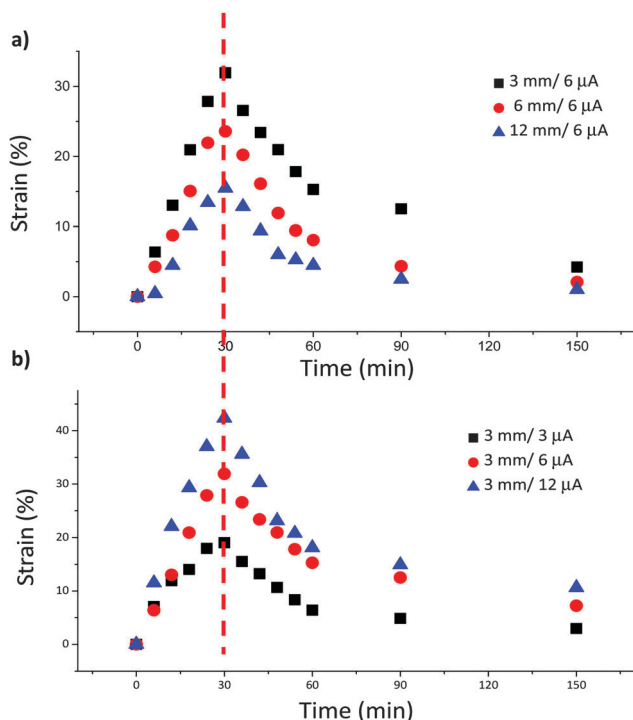


Fig. 4 Graphical illustration of strain changes in the micro PAA actuator with (a) varied inter-electrode distances and constant current magnitude (6 μA), and (b) varied current magnitudes and constant inter-electrode distance (3 mm). In all experiments, the ORR current is removed after 30 minutes, represented graphically by the red dashed line.

The more important impact, though, is that related to the magnitude of the pH gradient that leads to ionization of the PAA network. Sustaining this gradient against diffusive dissipation is essential to realizing large changes in strain. Experimental observations support this point, as varying the applied ORR current magnitudes between 3, 6, and 12 μA , with equal inter-electrode distances (3 mm) as a control, yielded maximum strain changes of 19.8%, 32.7%, and 43.2% respectively for the PAA micro strips (Fig. 4b, experimental images in Fig. S5, ESI[†]). These results show that the actuation response shows a positive correlation with the magnitude of the current, most likely because a higher current sustains a more pronounced flux of hydroxide ion in the region of the co-localized cilia. A full discussion of these tests can be found ESI[†], Section IV. The important point to take from these experiments is that the inter-electrode distances and current magnitudes are critical design parameters for tuning the chemomechanical responses of the PAA cilia.

3.5 ORR-induced chemomechanics of the macro PAA actuator

In order to replicate the electrochemical environment of the micro PAA actuator, the current density in the macro actuator experiments was maintained in approximately the same range as the micro actuator experiments (see ESI[†], Section V). In the macro PAA actuator design employed here (Fig. 5a), the embedded mesh electrodes were used as the cathode. A Au anode, along with a Au pseudo-reference electrode, was placed in the electrolyte solution away from the actuator. The protons consumed by the ORR at the cathode lead to ionization within the PAA gel network, which in turn drives the volumetric expansion of the gel. Fig. 5a-ii, shows the elongation of the macro PAA gel seen after sustaining the ORR current at this limit for 30 minutes (ESI[†], Movie S3). The expanded state of the gel fully relaxes after the ORR current is stopped (recovering completely after 30 minutes, Fig. 5a-iii, ESI[†], Movie S4). The plot in Fig. 5b shows the strain change of the PAA actuator measured through two cycles. Using the embedded electrodes as a fiduciary marker, we also note that a compensating (albeit small) compressive strain also appears to form in the direction transverse to the elongation noted above. This strain also relaxes when the current flow is stopped.

To ensure that the observed actuation is due to a response to a pH gradient, we fabricated a macro polyacrylamide (PAAm) actuator as a control. The non-ionogenic PAAm shows no pH sensitivity over the pH range of these experiments and a negligible dependence on the ion concentration in the solution.^{21,22} The PAAm control device, with the same open mesh embedded electrodes, shows no actuation response (ESI[†], Section VI and Fig. S6, ESI[†]) to an applied potential sufficient to drive an ORR current.

The macro PAA actuator shows a much smaller, albeit still reversible, strain change than the micro PAA cilia. With the increase of the solution volume (from 100 μL to ~ 10 mL electrolyte solution) and gel size (from ~ 0.02 to ~ 40 mm³), the generated pH gradient is less efficient in driving actuation, being subject to diffusive dissipation at a timescale faster than the stable range of operating currents can surmount. That larger/more macroscopic design rules are more resistant to

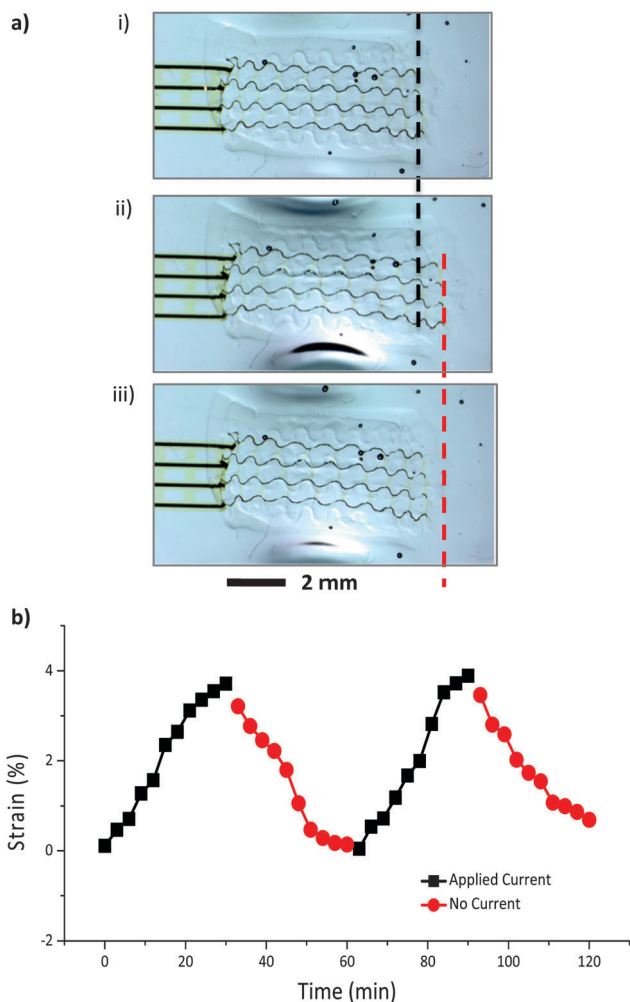


Fig. 5 (a) Optical image of the macro PAA actuator (i) before application of ORR current (the black dashed line indicates the end gel position of the actuator at $t = 0$ min), (ii) after application of ORR for 30 min (red dashed line indicates the end gel position of the expanded actuator at $t = 30$ min), and (iii) 30 min after removal of ORR current ($t = 60$ min). (b) Graphical illustration of the strain change of the macro PAA actuator throughout two cycles of application and removal of ORR current.

actuating material phase dynamics *via* electrochemical to mechanical energy conversion follows intuitive expectations for systems built around such operating mechanisms.

The most important exemplars that speak to this attribute of mechanism are in fact those afforded by living systems. Here one finds many examples where the superlative efficiencies of chemomechanical actuation come as much from the length scales of integration of system-level components (in which compartmentalization figures very importantly) as it does from the sophistication of the molecular systems supporting it. This suggests an important and motivating goal for future research to address.

4. Conclusions

In summary, we have fabricated and investigated composite ORR-induced chemomechanical hydrogel actuators. These actuators

undergo significant electrochemical to mechanical energy conversion. The micro PAA actuators demonstrate fast, largely reversible, actuation responses, and the macro PAA actuators demonstrate that this system can affect reversible actuation at much larger scales albeit, based on current modes of integration, with much diminished efficiencies. The actuation capabilities are determined by the mass (size) of the gel, inter-electrode distance, and current magnitude. Varying these parameters offers design rules for tuning the actuation output, but these parameters also demonstrate the effect of mass transfer on chemomechanical systems, both in actuation speed and magnitude. With precise control, these design rules, fabrication procedures, and integration of hydrogels and electronics lead to applications in biomimetic systems operable with an ORR trigger.

Acknowledgements

We (R. G. Nuzzo, J. A. Rogers, P. Yuan, and E. M. Erickson) gratefully acknowledge the support of the U.S. Department of Energy, Division of Materials Sciences under Award No. DE-FG02-07ER46471, through the Frederick Seitz Materials Research Laboratory at the University of Illinois at Urbana-Champaign. Additionally, C. M. Daly gratefully acknowledges the support of the U. S. Army Research Laboratory and the U. S. Army Research Office under grant number W911NF-13-0489.

References

- 1 S. K. Ahn, R. M. Kasi, S. C. Kim, N. Sharma and Y. X. Zhou, *Soft Matter*, 2008, **4**, 1151–1157.
- 2 K. Haraguchi and T. Takehisa, *Adv. Mater.*, 2002, **14**, 1120–1124.
- 3 R. V. Ramanujan and L. L. Lao, *Smart Mater. Struct.*, 2006, **15**, 952–956.
- 4 R. V. Martinez, C. R. Fish, X. Chen and G. M. Whitesides, *Adv. Funct. Mater.*, 2012, **22**, 1376–1384.
- 5 R. Yoshida, T. Takahashi, T. Yamaguchi and H. Ichijo, *J. Am. Chem. Soc.*, 1996, **118**, 5134–5135.
- 6 R. Yoshida, T. Sakai, S. Ito and T. Yamaguchi, *J. Am. Chem. Soc.*, 2002, **124**, 8095–8098.
- 7 M. Yamada, M. Kondo, J. I. Mamiya, Y. L. Yu, M. Kinoshita, C. J. Barrett and T. Ikeda, *Angew. Chem., Int. Ed.*, 2008, **47**, 4986–4988.
- 8 D. Schmaljohann, *Adv. Drug Delivery Rev.*, 2006, **58**, 1655–1670.
- 9 R. A. Siegel and B. A. Firestone, *Macromolecules*, 1988, **21**, 3254–3259.
- 10 I. C. Kwon, Y. H. Bae and S. W. Kim, *Nature*, 1991, **354**, 291–293.
- 11 K. Kontturi, S. Mafe, J. A. Manzanares, B. L. Svarfvar and P. Viinikka, *Macromolecules*, 1996, **29**, 5740–5746.
- 12 J. H. Holtz and S. A. Asher, *Nature*, 1997, **389**, 829–832.
- 13 T. Miyata, N. Asami and T. Uragami, *Nature*, 1999, **399**, 766–769.

- 14 T. Tanaka, I. Nishio, S. T. Sun and S. Ueno-Nishio, *Science*, 1982, **218**, 467–469.
- 15 T. Shiga and T. Kurauchi, *J. Appl. Polym. Sci.*, 1990, **39**, 2305–2320.
- 16 C. Yu, Z. Duan, P. Yuan, Y. Li, Y. W. Su, X. Zhang, Y. Pan, L. L. Dai, R. G. Nuzzo, Y. Huang, H. Jiang and J. A. Rogers, *Adv. Mater.*, 2013, **25**, 1541–1546.
- 17 S. M. Mitrovski, L. C. C. Elliott and R. G. Nuzzo, *Langmuir*, 2004, **20**, 6974–6976.
- 18 S. M. Mitrovski and R. G. Nuzzo, *Lab Chip*, 2005, **5**, 1184.
- 19 E. M. Erickson, S. M. Mitrovski, A. A. Gewirth and R. G. Nuzzo, *Electrophoresis*, 2011, **32**, 947–956.
- 20 M. R. Tarasevich, A. Sadkowsky and E. Yeager, Kinetics and mechanisms of electrode processes, in *Comprehensive Treatise of Electrochemistry*, ed. B. E. Conway, J. O. M. Bockris, E. Yeager, S. U. M. Khan and R. E. White, Plenum Press, New York, NY, USA, 1983, vol. 7, pp. 301–398.
- 21 J. Ricka and T. Tanaka, *Macromolecules*, 1984, **17**, 2916–2921.
- 22 P. Bonina, T. Petrova, N. Manolova and I. Rashkov, *J. Bioact. Compat. Polym.*, 2004, **19**, 197–208.